Journal of Magnetic Resonance 203 (2010) 156–166

Contents lists available at ScienceDirect

Journal of Magnetic Resonance

journal homepage: www.elsevier.com/locate/jmr

Optimized excitation pulses for the acquisition of static NMR powder patterns from half-integer quadrupolar nuclei

Luke A. O'Dell, Kristopher J. Harris, Robert W. Schurko *

Department of Chemistry and Biochemistry, University of Windsor, Windsor, Ont., Canada N9B 3P4

ARTICLE INFO

Article history:
Received 24 August 2009
Revised 27 November 2009
Available online 23 December 2009

Keywords:
Solid-state nuclear magnetic resonance
Half-integer quadrupolar nuclei
Optimal control theory
Signal enhancement
Population transfer

ABSTRACT

Various amplitude- and phase-modulated excitation pulses for the observation of static NMR powder patterns from half-integer quadrupolar nuclei have been generated using the optimal control routines implemented in SIMPSON 2.0. Such pulses are capable of both excitation of the central transition and signal enhancement by population transfer from the satellites. Enhancements in excess of 100% have been achieved for the central transition of the spin-3/2 ^{87}Rb nucleus compared with a selective $\pi/2$ pulse. These pulses are shown to be relatively insensitive to changes in RF power and transmitter offsets, and can achieve a more uniform signal enhancement than double-frequency sweeps (DFS), resulting in more accurate spectral lineshapes. We also investigate the possibility of "calibration-free" optimized pulses for general use on half-integer quadrupoles with unknown interaction parameters. Such pulses could prove extremely useful for studying low abundance or insensitive nuclei for which experimental optimization of the DFS scheme may be difficult. We demonstrate that a pulse optimized for an arbitrary spin-3/2 system can function well on multiple samples, and can also excite the central transition of higher spin numbers, albeit with a smaller enhancement. The mechanism by which these optimized pulses achieve the signal enhancement is highly complex and, unlike DFS, involves a non-linear excitation of the satellite transition manifold, as well as the generation and manipulation of significant multiple-quantum coherences.

1. Introduction

Nuclear magnetic resonance is an inherently insensitive spectroscopic technique due primarily to the very small population differences between the Zeeman energy levels of nuclear spins placed in an external magnetic field. A significant amount of NMR research is therefore focused on enhancing the signal attainable from NMR experiments. One way of improving sensitivity is to increase the efficiencies of spin-state manipulations (*e.g.*, transfer of the Zeeman population differences into observable single-quantum coherences) up to their maximum theoretical limits which are set by the universal boundaries on spin dynamics [1]. Achieving such optimization numerically has a substantial computational cost due to the extremely large number of variables involved in a typical NMR experiment, which describe the interactions affecting the spins, their response to any applied radiofrequency (RF) control fields, and dynamic effects such as magic angle spinning (MAS). Optimal control theory (OCT) is a mathematical tool capable of dealing with a system composed of a large number of variables which can be used to determine the optimum pathways between spin states, thereby maximizing experimental sensitivity. In the past few years, optimal control theory has been employed in numerous magnetic resonance applications, including NMR spectroscopy. Examples include improvements in coherence transfer [2–6], dipolar recoupling [7–11] and excitation of multiple-quantum coherences [12]. Recently, optimal control procedures have been implemented in version 2.0 of the open-source solid-state NMR simulation package SIMPSON [13,14], making optimal control easily accessible to the NMR community due to the simplicity of the SIMPSON interface. This should allow for the improvement of a very broad range of solid-state NMR pulse sequences, as well as the design of novel experiments. In this work, we have used SIMPSON to optimize excitation pulses for the observation of static, central transition NMR powder patterns from half-integer quadrupolar nuclei. To the best of our knowledge, optimal control theory has until now been applied only once to quadrupolar nuclei (spin $I > ½$) in the solid state, to improve triple-quantum excitation in the MQMAS experiment [12].

The low intrinsic sensitivity of NMR is exacerbated in the case of a static, powder sample due to various anisotropic interactions such as chemical shielding anisotropy (CSA), and in the case of quadrupolar nuclei, the coupling of the nuclear electric quadrupole moment with the surrounding electric field gradient (EFG). These interactions perturb the Zeeman energy levels to different extents depending on the relative orientation of the interaction tensor and

* Corresponding author. Fax: +1 519 973 7098.
E-mail address: rschurko@uwindsor.ca (R.W. Schurko).

1090-7807/$ - see front matter © 2010 Elsevier Inc. All rights reserved.
doi:10.1016/j.jmr.2009.12.016

the external magnetic field, resulting in powder patterns that are inhomogeneously broadened in the frequency domain, often over ranges that cannot be uniformly excited using conventional NMR techniques (*i.e.*, rectangular, monochromatic RF pulses). Even for relatively narrow powder patterns, the sensitivity of NMR experiments on quadrupolar nuclei may be further reduced by a low gyromagnetic ratio, a low natural abundance, a low quantity of the nucleus in question, or a combination of these factors. Nevertheless, such powder patterns are worthwhile to obtain since the anisotropic nature of these interactions can provide valuable information on the electronic structure surrounding the nucleus *via* the CSA and EFG tensors and their relative orientations, and in some cases can also allow molecular dynamics to be probed.

Previous excitation pulses generated using optimal control theory have been designed with high-resolution solution NMR in mind. Broadband excitation and inversion pulses (BEBOP/BIBOP [15–17]) have been developed with a focus on uniformly exciting or inverting the ^{13}C magnetization over the full chemical shift range at high magnetic field strengths (*ca.* 50 kHz). The best-performing BEBOP pulses are typically on the order of 500 μs or more in length, and can be restricted to relatively low maximum or mean RF field strengths (*ca.* 10 kHz) to avoid sample heating. They can also be optimized to account for RF inhomogeneity. Constant-amplitude "calibration-free" pulses have also been presented [18], as well as ICEBERG pulses that result in transverse magnetization with a constant phase dispersion as a function of offset frequency [19].

We herein present a variety of amplitude- and phase-modulated excitation pulses generated using SIMPSON 2.0, designed for the efficient acquisition of static central transition powder patterns from half-integer quadrupolar nuclei. These pulses are generally shorter in length and use higher RF powers than the BEBOP pulses mentioned above, and can result in not only uniform excitation of the central transition, but also significant signal enhancement. We investigate the advantages of these pulses, outline some of the practicalities in generating them, and compare their performance and function to another commonly used signal enhancement technique (double-frequency sweeps, DFS) [20]. We also discuss the potential of creating "calibration-free" excitation pulses for half-integer quadrupoles.

2. Experimental details

All optimized pulses were generated using SIMPSON 2.0.0 [14] running on an HP laptop computer with the Windows XP operating system. $RbClO_4$ was chosen as a model system on which to test the pulses, since ^{87}Rb is a receptive spin-3/2 nucleus and the central transition powder pattern of this sample shows visible contributions from both the quadrupolar interaction and chemical shielding anisotropy at 9.4 T. Unless otherwise stated, the NMR interaction parameters used in the pulse optimizations were $C_Q = 3.3$ MHz, $\eta_Q = 0.2$, $\delta_{CSA} = -10$ ppm, $\eta_{CSA} = 0.1$, $\alpha = 90°$, $\beta = 35°$ and $\gamma = 90°$; these are values based on a previously reported single-crystal study [21]. The transmitter frequency for the pulses was centred at the isotropic chemical shift. Powder averaging was achieved using 376 orientations for the pulse optimizations and 28,656 orientations for the simulated spectra, with orientations calculated using the Zaremba Conroy Wolfsberg (ZCW) method. Pulses were defined *via* their length (between 1 and 80 μs) and individual element size over which the RF amplitude and phase remain constant. The element sizes chosen for the pulses were 0.1 μs for pulses $\leqslant$10 μs in length, and 0.25 μs otherwise. This latter element size is small enough to allow RF modulations at offsets of up to 2 MHz from the transmitter frequency (the maximum offset frequency is given by $(2 \times \text{element length})^{-1}$), thus covering the full satellite transition manifold of ^{87}Rb in $RbClO_4$, which is around 3.5 MHz in width. Initial amplitudes and phases for each element were randomly assigned with an imposed limit on the maximum amplitude (*i.e.*, RF power) of 50, 100 or 150 kHz. For each pulse length and maximum RF amplitude, a range of initial, random shapes were optimized and tested experimentally in order to improve the chances of finding the global optimum (*vide infra*). For the optimization procedure itself, the exit tolerance was set to 10^{-4} on the target function and 10^{-3} on the line search, with an initial step size for the bracketing minimum of 10 [14]. In each step of the iteration procedure, a one-point FID was acquired using the I1c detection operator, with the optimization aiming to maximize its amplitude. Typically, optimizations took between 5 and 100 iterations and between 1 and 100 min to complete depending primarily on the number of pulse elements being optimized. The final pulse shapes were output as text files without any further treatment and converted manually into the P-Code format suitable for use with the Varian Spinsight software.

All experiments were conducted at 9.4 T on a Varian InfinityPlus spectrometer, with Larmor frequencies of 130.8 (^{87}Rb), 38.6 (^{85}Rb) and 91.7 MHz (^{45}Sc). A sample of rubidium perchlorate ($RbClO_4$) was synthesized following literature procedures [22], a sample of Rb_2SO_4 was purchased from Aldrich and a sample of anhydrous scandium trifluoromethanesulfonate ($Sc(OTf)_3$) was also synthesized following literature procedures [23]. A 4.0 mm HXY Varian T3 probe was used for all experiments. Rubidium NMR spectra were referenced against 1.0 M aqueous $RbNO_3$ (0.0 ppm) and ^{45}Sc NMR spectra against a dilute solution of >0.1 M $ScCl_3$ dissolved in 0.05 M HCl (0.0 ppm) [24]. One-pulse type sequences were used for ^{87}Rb and ^{45}Sc experiments (optimized pulse – receiver delay – acquire). The receiver delay was set to 15 μs for all experiments except those of ^{45}Sc (20 μs). For ^{85}Rb spectra, significant probe ringing combined with a short T_2^* necessitated the use of an echo sequence (optimized pulse – 0.5 ms delay – π – acquire), with a monochromatic π-pulse (100 kHz RF power) used to acquire the full echo, which was processed with a magnitude calculation after Fourier transformation. Optimized refocusing pulses are more difficult to generate than excitation pulses [14], and while we are currently investigating their potential, they will not be discussed here. CYCLOPS phase cycling was used in all cases, and, unless otherwise stated, the transmitter frequency was placed as close as possible to the isotropic chemical shift of the nucleus in question. All reported relative integrated signal intensities for ^{87}Rb in $RbClO_4$ were normalized to that obtained from a monochromatic $\pi/2$ pulse, at 25 kHz RF power to ensure central transition selectivity, unless indicated otherwise. For comparison purposes, double-frequency sweep (DFS) pulse sequences were also used [20], with experimentally optimized converging DFS waveforms (see Section 3.1 for details) followed by a 0.75 μs delay and finally a 1.25 μs $\pi/2$ pulse (*n.b.*: the final $\pi/2$ pulse itself was not optimized). Processing of spectra and Fourier analysis of the pulse shapes were carried out using the NUTS software. A DC offset correction was applied to all spectra prior to signal integration. Density matrix analysis was carried out using SIMPSON 2.0.0 [14].

3. Results and discussion

3.1. Pulse optimizations and experimental performance

Various examples of optimized ^{87}Rb central transition excitation pulses for the $RbClO_4$ sample at 9.4 T are shown in Fig. 1, with the maximum RF amplitude limited to 100 kHz in each case. Limitations were imposed on the RF power for two reasons: (i) a moderate maximum RF power will avoid possible equipment damage or sample heating, and (ii) we intend to eventually apply these types of pulses to low-γ nuclei such as ^{17}O, for which higher pow-

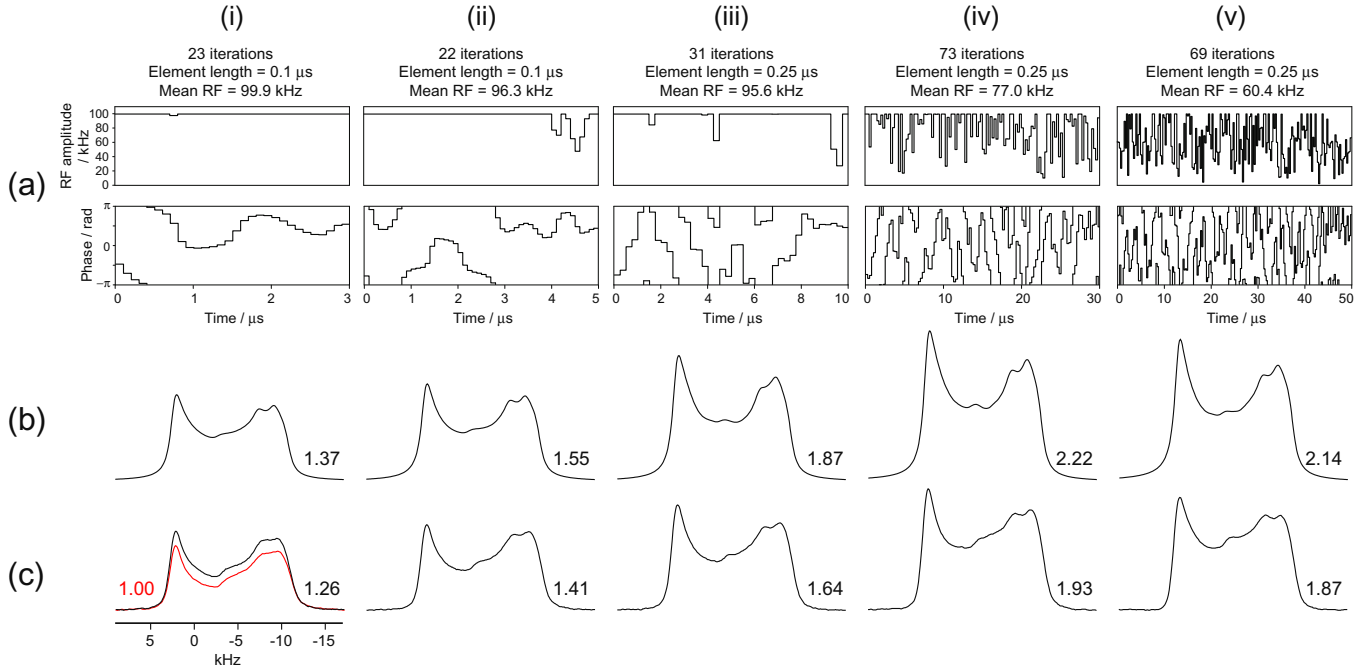

Fig. 1. (a) RF amplitude and phase profiles of pulses optimized for the excitation of the ^{87}Rb central transition of a static sample of $RbClO_4$ at 9.4 T, with a maximum RF amplitude of 100 kHz and pulse durations of (i) 3, (ii) 5, (iii) 10, (iv) 30 and (v) 50 µs. (b) Simulated spectra and (c) experimental spectra obtained from these pulses with relative signal enhancements shown, normalized to the spectrum arising from a 25 kHz monochromatic, central transition-selective $\pi/2$ pulse (this experimental spectrum is shown in red). Also shown at the top are the number of iterations taken in generating each pulse from a random initial shape, the individual element lengths and their mean RF powers. (For interpretation of color mentioned in this figure the reader is referred to the web version of the article.)

ers are more difficult to achieve. We stress that the removal of this restriction would allow greater freedom in the pulse optimization and would likely result in improved pulse performance at the cost of greater demands on RF power. As can be seen in Fig. 1, the extent of amplitude modulation clearly increases with longer pulse lengths, reflected in a decreasing mean RF power. The 50 µs pulse (Fig. 1v) shows a mean RF of just *ca.* 60% of the maximum permitted value. Conversely, significant phase modulation is observed even at relatively short pulse lengths, with the phase of the 3 µs pulse (Fig. 1i) being swept over the majority of the 2π range across its relatively short duration. At the end of each pulse the phase modulation terminates at *ca.* $\pi/2$ rad. Experimentally, these pulses show a level of performance that matches qualitatively with the simulations (Fig. 1b and c). The full ^{87}Rb powder pattern is fully excited in all cases, with the discontinuities arising from both the quadrupolar interaction and chemical shielding anisotropy clearly visible. The experimental signal intensities (shown in Fig. 1c and normalized to that obtained from a 25 kHz $\pi/2$ pulse) are slightly lower than those of the simulations (Fig. 1b), a fact which is likely due to experimental effects that were not accounted for during the optimization process, such as the limited probe bandwidth, the presence of RF inhomogeneity, the ability of the waveform generator to accurately reproduce the rapid amplitude and phase modulations, and relaxation effects. We note that SIMPSON 2.0 *is* capable of accounting for arbitrary RF inhomogeneity profiles and optimizing the pulses to compensate for them; however, after some initial testing we found that this did not seem to improve the experimental performance of the particular pulses studied here. It is likely that a longer element size would result in closer agreement between simulation and experiment since the pulse shapes would be easier for the spectrometer to reproduce accurately, and would also feature a narrower range of modulation frequencies, thus alleviating the effects of the limited probe bandwidth (at a cost of covering a narrower range of the satellite transition manifold, see Section 3.3). We also note that, unlike BEBOP pulses [15–17], these pulses are not scaleable.

The rapid amplitude and phase modulation seen in these optimized pulses indicates that they are operating at relatively large offsets from the transmitter frequency, *i.e.*, in the region of the satellite transitions. This is confirmed by the experimental signal enhancements shown in Fig. 2 (relative to a 25 kHz $\pi/2$ pulse), which could only arise *via* a population transfer mechanism from the satellite transitions. Significant signal enhancements are achieved even at relatively short pulse lengths, although the extent of enhancement increases with increasing maximum RF power and also with increasing pulse lengths (both in simulation and experiment), at least up to 30 µs. The 30 µs pulse with 150 kHz maximum RF power (mean RF power = 100.0 kHz) gave a signal enhancement of 112% (spectrum not shown), indicating at least

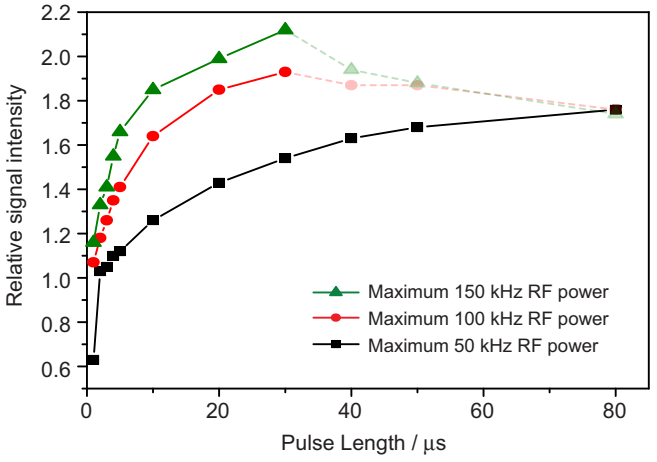

Fig. 2. ^{87}Rb experimental signal intensities obtained from a variety of optimized pulses of various lengths and maximum RF powers. Signal intensities are normalized to that obtained using a 25 kHz monochromatic, central transition-selective $\pi/2$ pulse. Faded points represent pulse lengths for which the optimal solution was not found.

partial inversion of the satellite transitions. (*n.b.*: The maximum theoretical enhancement arising from population transfer for the central transition of a spin-*I* nucleus is *I* + ½ for satellite transition saturation and 2*I* for full, sequential satellite inversion). At pulse lengths longer than 30 μs, enhancements decreased in both experiment and simulation for the 100 and 150 kHz limits; thus, these pulses are clearly not optimal solutions. This is due to the optimization process terminating at a *local* solution. It is clear that, for example, a 50 μs pulse must exist that performs at least as well as the 30 μs pulse (a trivial example would be a 20 μs delay followed by the very same 30 μs pulse). Global solutions become increasingly difficult to locate as the pulse lengths and maximum RF powers are increased due to the ever-increasing size of the variable space through which the optimization must search, as well as the increased abundance of local solutions. The apparent convergence of experimental signal intensities to *ca.* 1.75 for the three 80 μs pulses in Fig. 2 is therefore misleading, perhaps indicative of a large family of locally-optimum pulses that lead to this particular level of enhancement. Note that each point in Fig. 2 represents the experimental signal intensity achieved by the best-performing pulse of between 5 and 10 optimized pulses, each of which was optimized from a different initial random shape. It is expected that a larger number of such optimizations would eventually find pulses that yield greater signal enhancements for the >30 μs pulses, however, Fig. 2 suggests that finding the true global optimum at longer pulse lengths and higher RF powers would likely be a case of diminishing returns, with smaller and smaller improvements achievable at an ever-increasing cost in terms of the number of optimizations to perform and test. Relaxation effects would also be likely to play a detrimental role in the experimental performance of longer pulses.

The possibility of enhancing the central transition signal from half-integer quadrupoles by population transfer from the satellites has been established for a long time [25,26], with various reported methods available for both static and MAS experiments [20,27–30], and a recent example of an analogous signal enhancement mechanism that can be exploited in integer spin systems [31]. We tested the performance of the 30 μs, 100 kHz optimized pulse in Fig. 1iv (hereafter referred to as the KP pulse, having been optimized using the known parameters for $RbClO_4$) against the DFS method, a well-established and commonly used enhancement mechanism for static quadrupolar samples (see Fig. 3). This particular optimized pulse was chosen for its excellent experimental performance (93% experimental signal enhancement) and modest maximum and mean RF powers (100.0 and 77.0 kHz, respectively). Its performance was compared to two different DFS – $\pi/2$ pulse se-

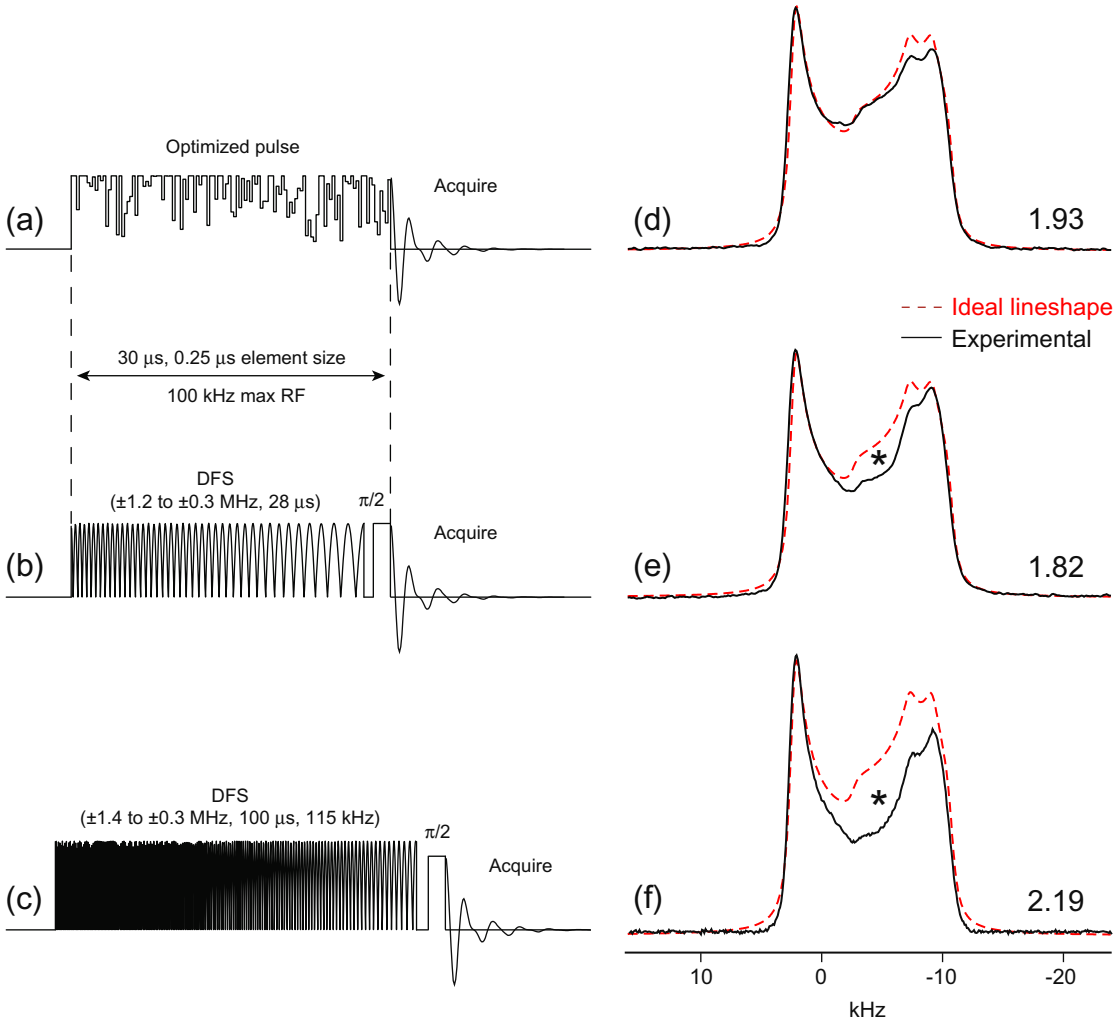

Fig. 3. A comparison of (a) an optimized excitation pulse with (b) a DFS – $\pi/2$ pulse sequence restricted to the same length, power and element size and (c) an unrestricted DFS sequence (not to scale, see text for discussion). The DFS parameters were optimized experimentally. The resultant ^{87}Rb experimental spectra are shown in (d), (e) and (f), respectively, along with the relative signal intensities. The ideal lineshapes (shown in red) were generated using SIMPSON. The asterisks in (e) and (f) indicate the "magic angle region" (see text for discussion). (For interpretation of color mentioned in this figure the reader is referred to the web version of the article.)

quences, the first restricted for the sake of comparison to a total length of 30 μs, a resolution (*i.e.*, element length) of 0.25 μs, and a maximum RF power of 100 kHz, *i.e.*, identical restrictions to those placed on the KP pulse (Fig. 3b), and the second unrestricted in length and RF power (Fig. 3c). These are hereafter referred to as the "restricted" and "unrestricted" DFS – $\pi/2$ pulse sequences, each having been optimized *experimentally* by extensive manual adjustment of the various parameters in order to maximize the observed signal. The final parameters used for each sequence are shown in Fig. 3. Note that the adiabaticity factor A for the DFS waveform is given by $(\nu_1{}^2\cdot\tau)/(\nu_i - \nu_f)$ for a static sample, where ν_1 is the RF nutation frequency, τ is the duration of the sweep, and ν_i and ν_f are the initial and final offset frequencies, respectively. The adiabaticity of the restricted DFS waveform is therefore 0.31 (sudden passage) whereas for the unrestricted waveform is 1.2 (adiabatic passage), thus the latter would be expected to be more likely to achieve inversion of the satellite transitions and thus a greater signal enhancement. All three pulse sequences achieved a considerable signal enhancement, and the unrestricted DFS sequence produced the highest signal intensity of 2.19, albeit with significant distortion of the powder pattern from its ideal shape (Fig. 3f). The KP pulse produced a signal intensity of 1.93 (compared with 1.82 for the restricted DFS sequence) as well as the most accurate lineshape of the three experiments, with a particular improvement in the region of the pattern corresponding to crystallite orientations where the principal axis of the EFG tensor (*i.e.*, the direction of the largest EFG tensor component, V_{33}) is aligned close to the magic angle (54.74°) with respect to the external field (this region is marked with an asterisk in Fig. 3). The DFS sequences would be expected to be less effective at enhancing this region of the powder pattern due to the relatively close proximity of the central and satellite transition frequencies for these crystallites. Despite a similar distortion appearing in the *simulated* spectrum of the KP pulse (see Fig. 1b(iv)), the pulse appears to result in a more uniform enhancement in this region of the experimental pattern than the DFS sequences. This is a potentially important advantage of the KP pulse over DFS, as lineshape accuracy is crucial if accurate CSA and EFG tensor parameters (and relative orientations) are to be extracted from the static spectrum. In order to understand how the KP pulse might enhance this "magic angle region" more effectively than the DFS sequence, we conducted both density matrix and time-resolved Fourier transform analysis in an attempt to shed light on the differences in the mechanisms by which the two pulse sequences excite the satellite transitions. This analysis is discussed in Section 3.3.

We note that in recently published work [32], a long (>10 ms), low power DFS – $\pi/2$ pulse sequence was optimized using OCT with the aim of enhancing the ^{23}Na central transition signal and suppressing the satellites in solution and liquid-crystalline samples (the same authors went on to use OCT to create pulses which compensate for relaxation effects [33]). Such long sweep durations at lower RF powers should also be advantageous in solid, powder samples to avoid unwanted double-quantum transitions [30]. We also note that the use of long, adiabatic hyperbolic secant (HS) inversion pulses can also result in very significant signal enhancement in static samples [34], although these pulses were not investigated in this work. Optimized pulses of this length will be more difficult to generate from a random initial shape due to the vastly increased number of pulse elements. It therefore seems likely that the generation of pulses that can achieve maximum theoretical enhancements (as well as minimal lineshape distortions) will most easily be achieved using DFS or HS sequences as a starting point for the optimization. SIMPSON 2.0 is capable of taking any arbitrary pulse sequence as an initial shape to optimize, and so we conducted an optimization of the restricted DFS – $\pi/2$ sequence (Fig. 3b); however, the resulting pulse did not show an improved experimental performance in this instance (spectrum not shown). We are currently pursuing this. The unrestricted DFS sequence in Fig. 3c gave rise to the largest integrated intensity observed in this study (119%, but only after extensive experimental optimization), an enhancement in agreement with a previous ^{87}Rb DFS study of $RbClO_4$ [22], albeit with significant lineshape distortion. The highest enhancement obtained with an optimized pulse was 114%, which was obtained using a 30 μs pulse that was limited in the optimization to 150 kHz but applied experimentally at 159 kHz. We stress that this does not imply a maximum possible enhancement attainable with optimized pulses, merely the highest observed in this preliminary study, and that longer pulses that can achieve greater enhancements will certainly exist.

3.2. Optimized excitation pulses for general use

Thus far we have discussed the performance of the KP pulse which was optimized with an *a priori* knowledge of the ^{87}Rb interaction parameters, and shows an excellent experimental performance on the system for which it was optimized, notably in the accuracy of the resultant lineshape. A question that must be addressed is whether or not such a pulse will have any use beyond the sample for which it was optimized, or must new RF pulses be optimized for each distinct sample? Moreover, can we create a pulse that gives rise to uniform excitation and signal enhancement in the general case of a spin-3/2 nucleus? In order to address the former question, we compared the performance of the KP pulse with a pulse optimized using the same RF power and length restriction, but with an arbitrary set of interaction parameters (C_Q = 5.0 MHz, η_Q = 0.0 and zero CSA), denoted as the AP (arbitrary parameters) pulse. These pulses are shown in Fig. 4, the AP pulse having a higher mean RF power of 85.0 kHz compared with 77.0 kHz for the KP pulse. Experimentally, the AP pulse excites the ^{87}Rb central transition powder pattern of $RbClO_4$, and gives rise to a significant experimental signal enhancement of 86% and a powder pattern that very closely matches the ideal shape. This clearly demonstrates that such optimized excitation pulses are not necessarily limited in their use to the exact spin systems for which they have been optimized.

Despite having been generated using an arbitrary set of interaction parameters, the AP pulse has nonetheless been optimized for use at a very specific transmitter frequency (*i.e.*, the isotropic shift of a C_Q = 5.0 MHz, η_Q = 0.0 powder pattern) and a specific RF power (100 kHz). If these pulses are to be applied to a sample with an unknown isotropic chemical shift, the transmitter frequency will inevitably be offset from this. We therefore tested the sensitivity of the AP pulse (as well as the KP pulse, the restricted DFS – $\pi/2$ sequence and a 100 kHz monochromatic $\pi/2$ pulse) to variations in the transmitter frequency and RF power, using the $RbClO_4$ sample. Fig. 5a shows the relative signal intensities obtained with these pulses at a range of offsets from the isotropic frequency (the probe having been retuned in each case). Clearly, the three signal enhancement schemes show a comparable performance over a 140 kHz range of transmitter frequencies. As one would expect, the KP pulse produces the strongest signal when applied at the isotropic frequency, since the experimental conditions in this case are exactly those for which the pulse was optimized. However, the KP pulse (as well as the restricted DFS – $\pi/2$ pulse sequence) appears to be much more sensitive to relatively small variations in the transmitter offset than the AP pulse, which was optimized for a larger C_Q value, and therefore a wider frequency distribution (*e.g.*, the KP pulse shows a noticeable drop in performance at an offset of −20 kHz). Fig. 5b compares the four experiments in terms of sensitivity to variations in the RF power. Interestingly, the AP pulse and DFS sequence show profiles that seem to be offset, actually performing better at a slightly higher RF power (this was also ob-

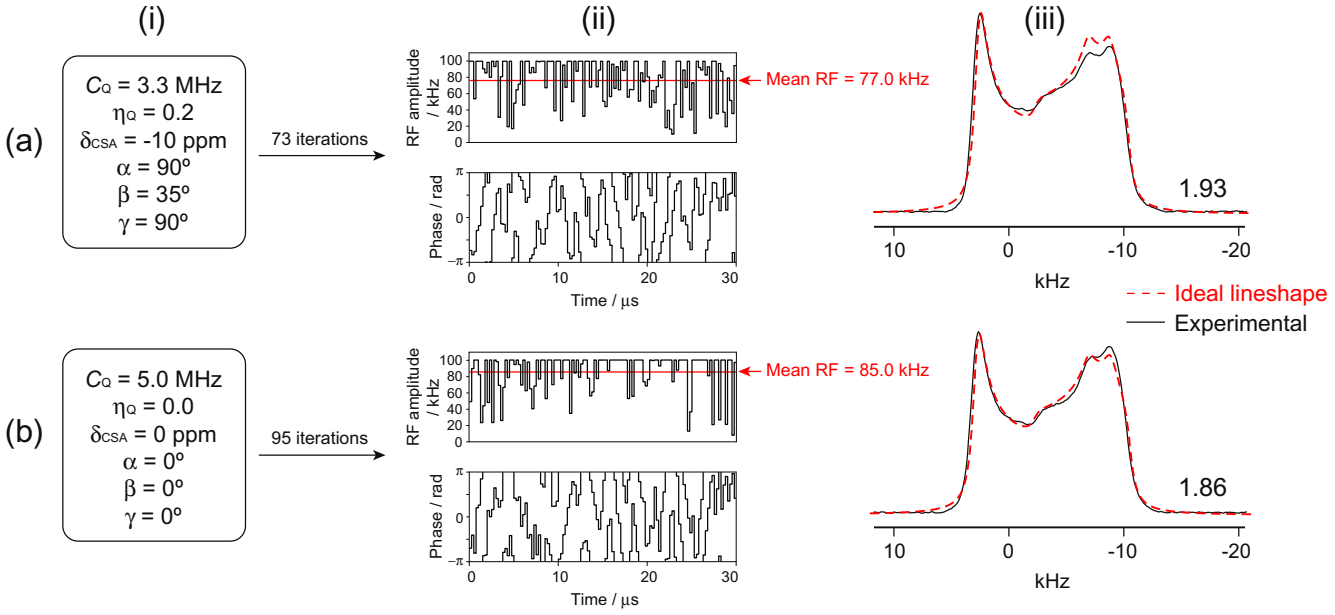

Fig. 4. (a) A known parameter (KP) optimized pulse generated using the ^{87}Rb NMR parameters for $RbClO_4$ and (b) an arbitrary parameter (AP) optimized pulse with a C_Q of 5.0 MHz specified in the optimization. The parameters used for the optimizations are given in (i), amplitude and phase profiles of the resultant pulses are shown in (ii) and the experimental spectra are shown in (iii) along with the relative signal intensities.

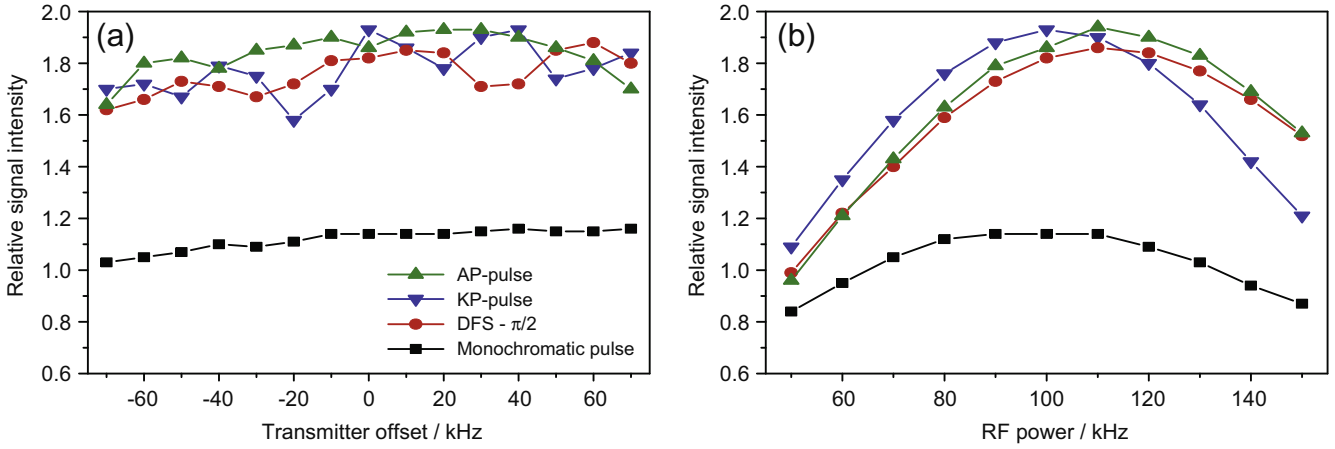

Fig. 5. Relative ^{87}Rb experimental signal intensities obtained from $RbClO_4$ using the arbitrary parameter (AP) and known parameter (KP) optimized pulses over (a) various transmitter offsets (relative to the ^{87}Rb isotropic shift) and (b) various RF powers (note that both AP and KP pulses were optimized to be applied at the isotropic shift at 100 kHz RF power). For comparison, results from the restricted DFS – $\pi/2$ sequence and a 100 kHz monochromatic $\pi/2$ pulse are also shown. Intensities are normalized to that obtained using a 25 kHz monochromatic, central transition-selective $\pi/2$ pulse.

served for certain other optimized pulses, not shown). At lower powers, the performance of the AP, KP and DFS schemes are comparable; however, at higher powers the decrease in signal for the AP and DFS sequences is less severe than for the KP pulse. We note that the accuracy of the lineshapes generally deteriorated with increasing offset frequency or power missets for all four sequences.

As a further test of the versatility of the AP pulse, we applied it to a sample of Rb_2SO_4, which features two rubidium sites with very different C_Q values (2.8 and 5.7 MHz, note that the latter value is larger than the C_Q for which the AP pulse was optimized). The other ^{87}Rb interaction parameters for Rb_2SO_4 can be found in reference [35]. The restricted DFS – $\pi/2$ sequence and 100 kHz monochromatic $\pi/2$ pulse were also applied to this system for comparison, and these spectra are shown in Fig. 6a, along with SIMPSON simulations in 6b. Both the AP pulse and DFS sequence produced different enhancements for each rubidium site, with a greater enhancement for the low C_Q site. This difference is due mainly to the C_Q values of the two sites, which result in very different frequency ranges for the satellite-transition manifolds of each site, and thus different population transfer efficiencies (the difference in isotropic chemical shifts will also play a role). Experimentally, the difference in enhancements produced by the AP pulse for each site is more significant than for the DFS sequence. This implies that the enhancement arising from the AP pulse is more dependent on the quadrupolar parameters of the sample than DFS, though the very similar enhancements in the simulations (Fig. 6b) suggest otherwise. This discrepancy between the experimental and simulated enhancements is likely due to experimental factors mentioned in Section 3.1 which are not accounted for in the simulations. Nonetheless, both sequences produced significant enhancements for both sites despite not having been optimized for Rb_2SO_4, and it is already well known that caution should be

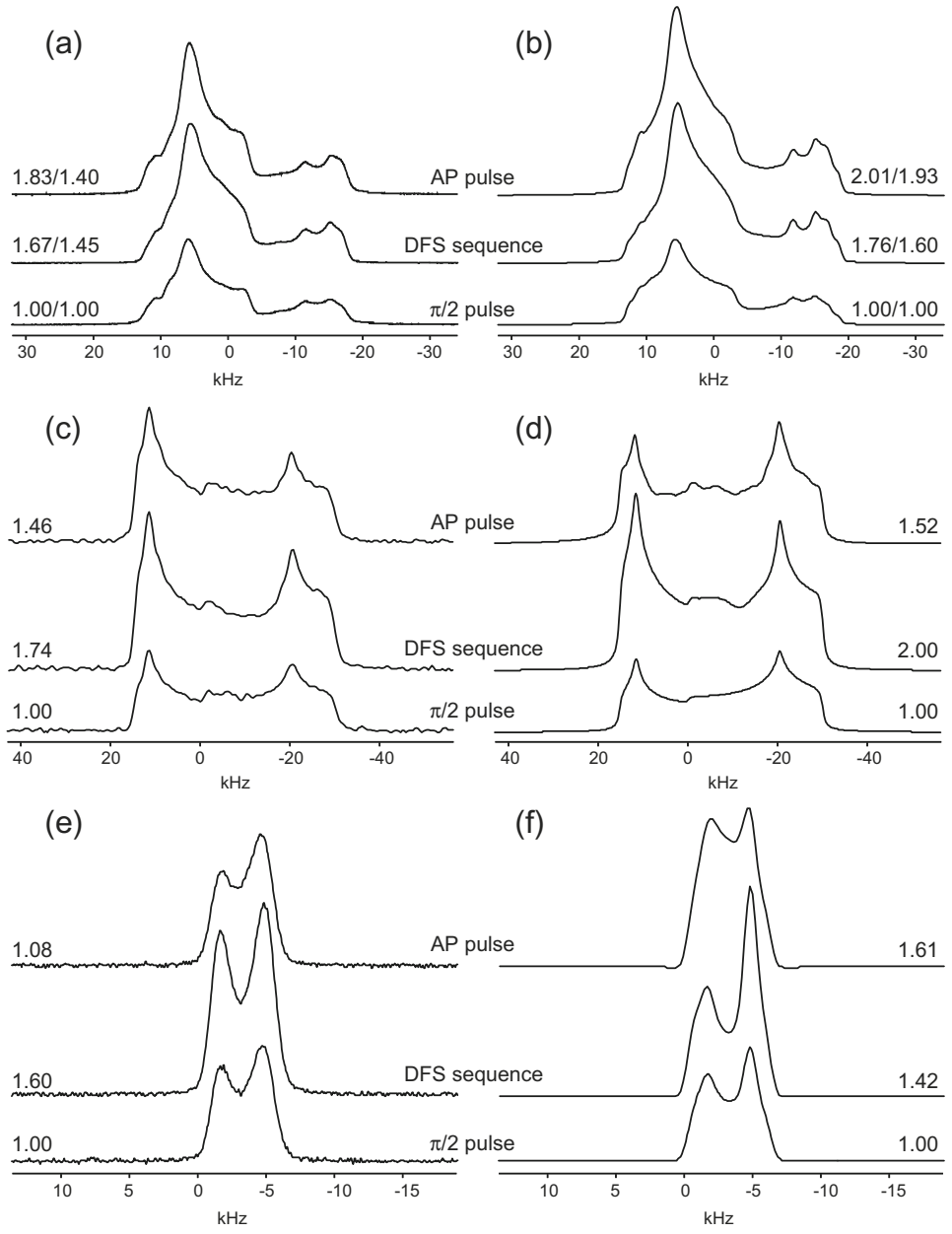

Fig. 6. Experimental (a, c and e) and simulated (b, d and f) spectra obtained using the AP pulse and the (unaltered) restricted DFS sequence applied at 100 kHz RF power. Signal enhancements are shown relative to a 100 kHz monochromatic $\pi/2$ pulse (also shown). (a) and (b) ^{87}Rb of Rb_2SO_4, (c) and (d) ^{85}Rb of $RbClO_4$ and (e) and (f) ^{45}Sc of $Sc(OTf_3)$. In (a) and (b), the relative intensities for the two individual sites in of Rb_2SO_4 are shown individually (the smaller C_Q site on the left and the wider pattern from the larger C_Q site on the right).

taken in interpreting spectra with multiple sites in a quantitative manner when such signal enhancement schemes have been used.

We have therefore demonstrated that optimized pulses can be created which both excite and enhance the central transition magnetization while functioning adequately over a range of interaction parameters, transmitter frequency offsets and missetting of the RF power. The AP pulse should therefore be useful for studying low-γ or low natural abundance spin-3/2 nuclei such as ^{33}S, providing both excitation and enhancement with very few parameters to adjust. The DFS enhancement scheme can be difficult to optimize experimentally on such nuclei, having a large number of parameters to vary (the initial/final offset frequencies, power and sweep rate of the DFS waveform, as well as the RF pulse used to excite the enhanced central transition magnetization, which has recently been shown to require more careful consideration than previously thought [36]). But what about variations in nuclear spin number? Is it possible to create a single pulse shape that can achieve central transition enhancement for any half-integer quadrupolar nucleus, or must the pulses be optimized separately for different nuclear spins? A single pulse shape optimized for general use would be extremely useful for transferring to low sensitivity or low natural abundance nuclei with higher spin numbers, such as ^{17}O. We tested the AP pulse and restricted DFS – $\pi/2$ sequence on two other spins (^{85}Rb and ^{45}Sc), in each case applying the sequence at 100 kHz RF power *with no further optimization*. While the performance of the DFS sequence could of course be improved by adjusting the experimental variables associated with the DFS waveform (just as the AP pulse could potentially be re-optimized for a new spin number), this particular experiment was intended to compare the "calibration-free" transferability of each sequence. Despite the

greater spin number of ^{85}Rb ($I = 5/2$) and relatively large ^{85}Rb C_Q of 6.7 MHz in $RbClO_4$, the AP pulse achieved an enhancement of 46% for this nucleus (Fig. 6c), with the full *ca.* 50 kHz width of the lineshape excited. The pulse also achieved a uniform excitation of the ^{45}Sc ($I = 7/2$) powder pattern in a sample of $Sc(OTf)_3$, albeit with a signal enhancement of only 8% (Fig. 6e). As with the $RbClO_4$ experiments, the DFS sequence resulted in a greater signal enhancement in both cases but at the expense of a more noticeable lineshape distortion away from the ideal (see the $\pi/2$ pulse simulations in Fig. 6d and f). We note the disparity between the experimental and simulated performance of the AP pulse on the ^{45}Sc sample, as well as the highly distorted simulated ^{45}Sc DFS lineshape in Fig. 6f. These are further examples of the limitations of such simulations in neglecting experimental factors such as probe bandwidth.

Considering that the maximum theoretical central transition enhancement for a spin-I nucleus is $2I$ (sequential inversion of satellite transitions from the outside in), it is clear that a re-optimization of the AP pulse for the higher spin numbers should be highly advantageous, and we are currently investigating this. However, the fact that the AP pulse can excite and enhance the central transition on different spin systems is highly encouraging, and illustrates the great potential of optimized excitation pulses for half-integer quadrupoles. As mentioned above, an optimized pulse, fixed in terms of its length, amplitude and phase modulation, that can achieve both excitation *and* enhancement of the central transition for any half-integer quadrupole would be much easier to apply to "difficult" samples due to the significantly reduced number of experimental parameters to adjust compared with other schemes such as DFS. However, we present this particular AP pulse as a proof-of-concept rather than a final product. While this pulse indeed produces an enhancement for three distinct spin numbers, the potential signal enhancements available in the higher spin systems should be considerably higher due to the greater number of satellite transitions. Optimization of pulses for higher spin numbers therefore appears crucial, although the size of the variable space through which the optimization procedure must search will be significantly larger due to the increased dimensions of the density matrix, which may increase the likelihood of optimizations terminating at local solutions. It seems clear that rather than searching for a single "cure-all" pulse that can be applied to any sample, the best course of action will be to produce a family of pulses, each of which works well on a specific spin number and over a certain range of C_Q values. Compromises between the extent

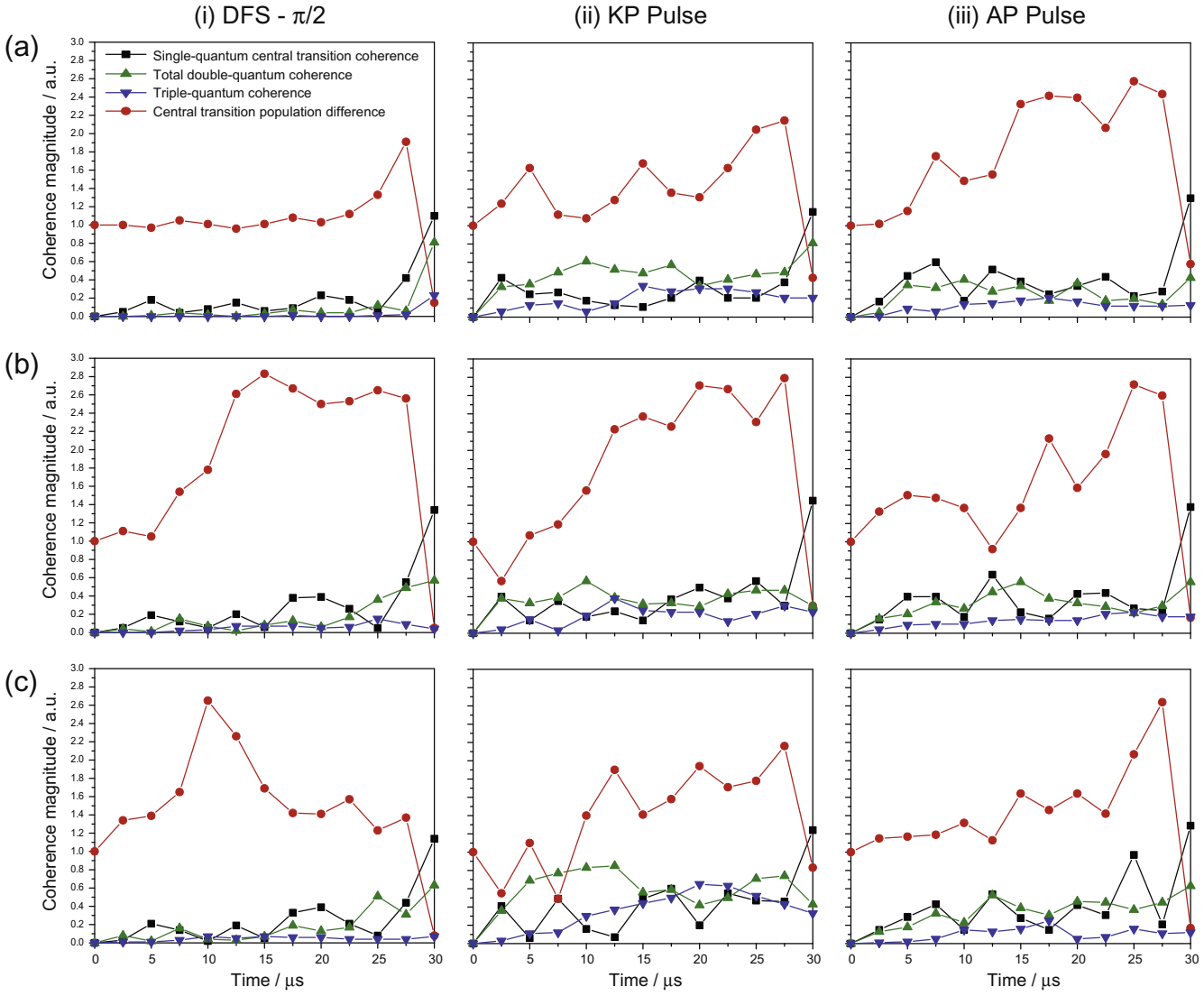

Fig. 7. Simulated evolution of ^{87}Rb single-, double- and triple-quantum coherences and the central transition population difference during (i) a DFS – $\pi/2$ sequence, (ii) a pulse optimized using known parameters (KP) and (iii) a pulse optimized using arbitrary parameters (AP) for a single crystal with the principal component of the EFG tensor oriented at (a) 54.74°, (b) 0° and (c) 90° relative to the external magnetic field.

of signal enhancement, robustness to transmitter offsets and lineshape accuracy may be required (the latter factor appears to be the biggest advantage of these optimized pulses over other schemes), and nuclei with lower gyromagnetic ratios or experiments conducted at lower magnetic fields will require pulses with greater restrictions placed on their maximum RF power. Establishing such pulses will clearly require a considerable amount of testing, though the above work demonstrates their potential.

3.3. How do the optimized pulses work?

In order to understand how the optimized pulses might produce a more uniform signal enhancement than the DFS experiment, particularly in the "magic angle region" of the ^{87}Rb powder pattern of $RbClO_4$ (see Fig. 3), we simulated the KP and AP pulses and the restricted DFS experiment and extracted the density matrices at various points in time during the application of the pulses. The single-quantum CT coherence magnitude was extracted *via* density matrix element ρ_{23}, the total double-quantum coherence from the sum of elements ρ_{13} and ρ_{24}, the triple-quantum coherence from element ρ_{14}, and the CT population difference from the difference between elements ρ_{22} and ρ_{33}. Plots of the density matrix evolution are shown in Fig. 7a for a crystallite with the largest principal axis of the EFG tensor oriented at $\beta = 54.74°$ with respect to the applied magnetic field (and, therefore, satellite transition frequencies in close proximity to that of the central transition). Towards the end of the DFS pulse (Fig. 7a(i)), the population difference across the central transition is seen to increase, despite the fact that the converging DFS waveform terminates at offsets of ±0.3 MHz (*vide infra*). The $\pi/2$ pulse subsequently converts this population difference into single and multiple-quantum coherences. Such multiple-quantum coherences are essentially absent during the application of the DFS waveform (*i.e.*, during the first 28 μs); however, this is not so for the KP and AP pulses (Fig. 7(ii) and (iii)), which create significant double- and triple-quantum coherences from their very beginning, and cause a less predictable, fluctuating variation in the central transition population difference over their duration. The final density matrices at the end of all three simulations in fact show very similar distributions in populations and coherences for the magic angle crystallite; however, the route that each sequence has taken in manipulating individual matrix elements is clearly very different. It is possible that the mechanism by which the optimized pulse might lead to a greater experimental signal enhancement in the "magic angle region" than the DFS sequence is *via* the excitation of these multiple-quantum coherences and their subsequent conversion to single-quantum, central transition coherence. Fig. 7 certainly serves to highlight the flexibility of the optimal control approach in terms of finding the optimal spin manipulation pathway among many possible routes.

For the $\beta = 0°$ crystallite, the DFS waveform enhances the CT population difference at an earlier point in time than for the magic angle crystallite (as would be expected given the increased offset of the ST frequencies from the CT) and this increased population difference is maintained until the application of the $\pi/2$ pulse (Fig. 7b(i)). However, for the $\beta = 90°$ crystallite the enhanced CT population difference is lost during the latter half of the DFS pulse sequence (Fig. 7c(i)). In contrast to this, the optimized pulses (Fig. 7(ii) and (iii)) appear to build up the CT population difference more steadily during their application. In particular, the AP pulse achieves consistently large CT population differences for all three crystal orientations, which may explain its improved insensitivity to transmitter offset. We do stress, though, that these simulations are only representative of three crystallite orientations, and that further simulations combined with single-crystal experiments should yield a more reliable insight into the mechanisms at play here.

An alternative approach to density matrix analysis for investigating the function of these experiments is to apply a Fourier transform (FT) to the pulse shapes themselves in order to determine the frequency distributions of the amplitude and phase modulations. Fig. 8 shows FTs of the DFS and optimized pulse shapes (after magnitude calculation) along with a simulation of the ^{87}Rb satellite transitions for visual reference. The FT of the 28 μs DFS waveform in Fig. 8b shows the symmetric regions of the satellite transitions over which the DFS pulse is swept (±1.2 to ±0.3 MHz), and the tailing of these features towards the transmitter frequency (0 MHz offset) may explain the non-zero enhancement of the CT population difference for the magic angle crystallite observed in Fig. 7a(i). In contrast, the FTs of the KP and AP pulses, in Fig. 8c and d, respectively, are asymmetric and "noisy", although they do superficially resemble the FT of the DFS waveform, with most of their intensity existing in the satellite regions, and a noticeable dip at zero offset where the central transition is located. These FTs do not, however, provide any intuitive sense of how the optimized pulses are operating. Time-resolved analysis was therefore performed by splitting the experiments into 2.5 μs pieces, Fourier transforming these individually, and constructing two-dimensional plots (Fig. 9). The plot for the DFS pulse sequence in Fig. 9a illustrates the converging DFS waveform as it traverses the satellite transition regions, and some intensity is present at zero offset at the end of the pulse sequence arising from the final $\pi/2$ pulse applied at the transmitter frequency. In sharp contrast, the plots for the optimized pulses reveal a rather chaotic mechanism with a seemingly random distribution of amplitude and phase modulation frequencies over the

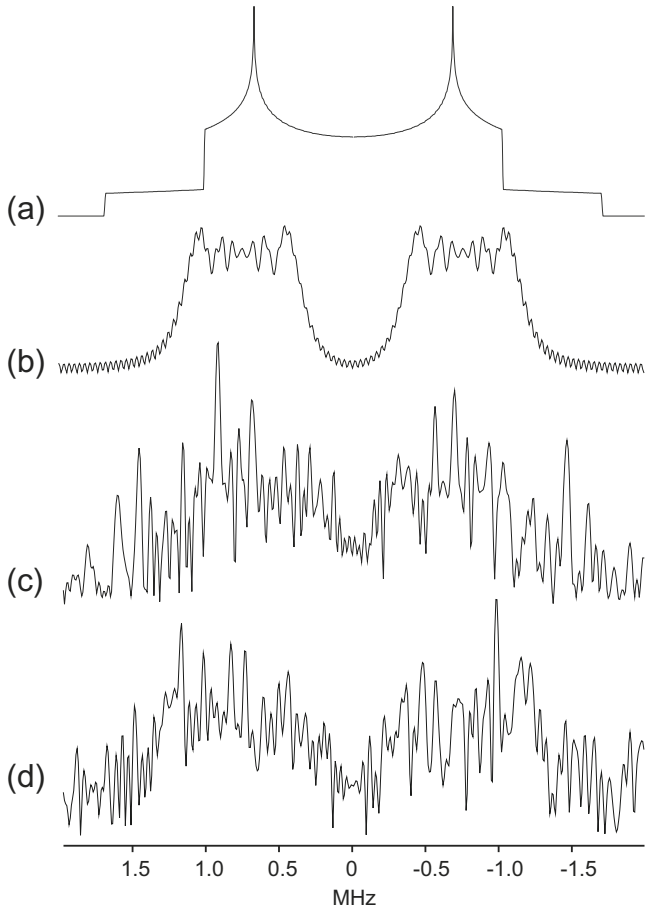

Fig. 8. (a) The satellite transition powder pattern for an ^{87}Rb nucleus with $C_Q = 3.3$ MHz and $\eta_Q = 0.2$ at 9.4 T, and the Fourier transformations (after a magnitude calculation) of (b) a DFS waveform 28 μs in length and swept between ±1.2 and ±0.3 MHz offsets, (c) the KP pulse and (d) the AP pulse.

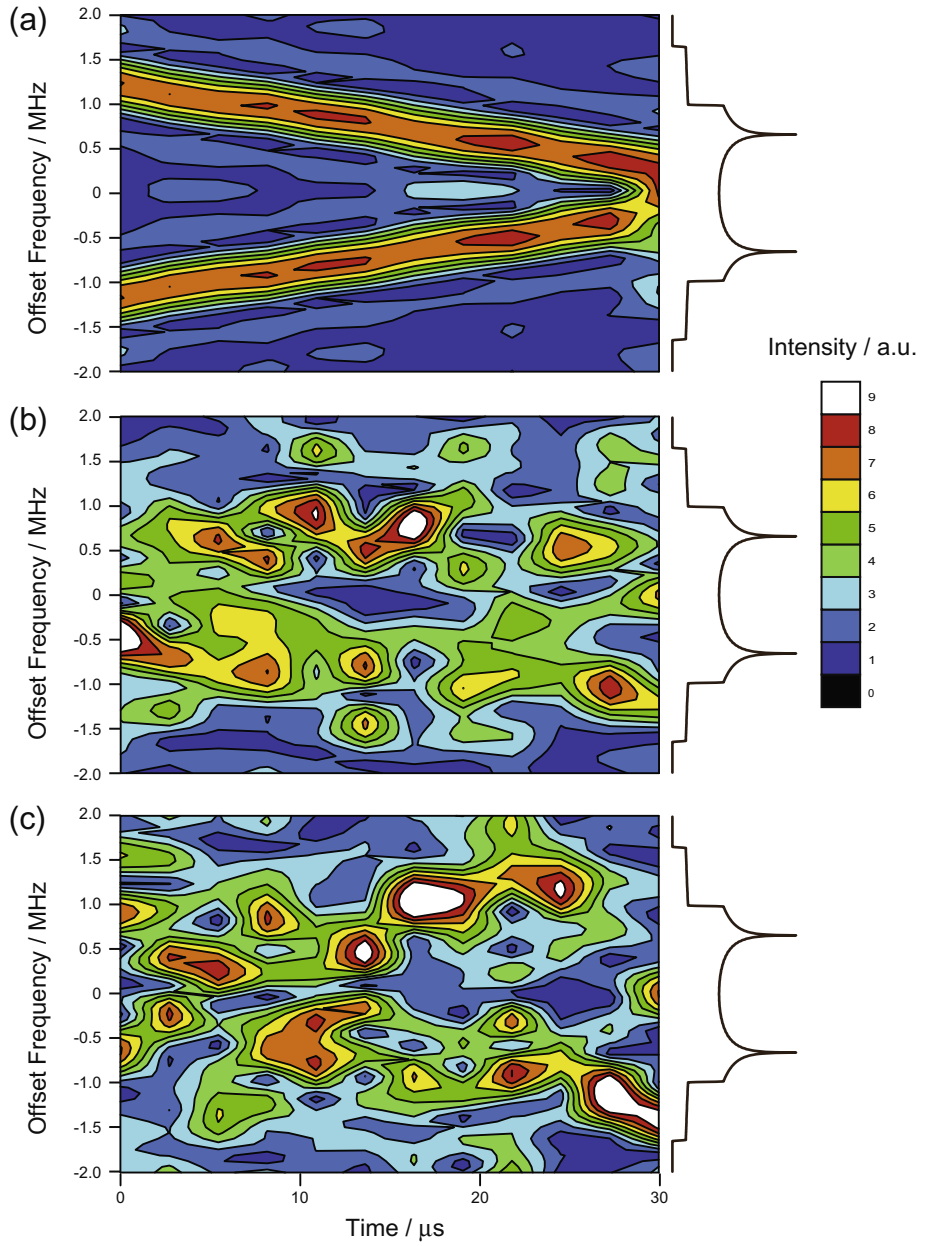

Fig. 9. Piecewise Fourier transformation analysis of (a) the 30 μs DFS – $\pi/2$ pulse sequence, (b) the KP pulse and (c) the AP pulse. The satellite transition powder pattern for an ^{87}Rb nucleus with C_Q = 3.3 MHz and η_Q = 0.2 at 9.4 T is shown to the right of each figure.

duration of the pulses (Fig. 9b and c). Upon close inspection, however, several observations can be made. Like the DFS – $\pi/2$ sequence, both optimized pulses show intensity at zero offset at the end of the pulse, representing the actual excitation of the central transition (*i.e.*, the conversion of the enhanced population differences into single-quantum coherences as seen in Fig. 7). Also like the DFS sequence, relatively little intensity occurs at zero offset over most of the pulse. This suggests that the majority of the pulse duration is spent manipulating the satellite transitions while leaving the central transition largely untouched. In fact, there appears to be less modulation at zero offset across the duration of the AP pulse than that of the KP pulse. Coupled with the fact that the FT of the AP pulse appears to show higher intensity at larger offset frequencies (see Fig. 8c and d), this may explain the improved tolerance of the AP pulse to offsets in the transmitter frequency discussed in Section 3.2. Unlike DFS, the excitation of the satellite transition regions by these optimized pulses is clearly extremely non-linear, and they appear to operate over a wider range of frequencies, thus covering the full satellite transition manifold (we note that when the DFS waveform was experimentally adjusted to cover a wider frequency range, the resultant spectra showed a reduced enhancement, and in some cases more severe lineshape distortion).

Figs. 7–9 seem to suggest that an intuitive understanding of the function of these optimized excitation pulses for half-integer quadrupolar nuclei may not be possible. Nonetheless, the ease with which these pulses can be generated and applied, coupled with their favourable experimental performance, particularly in terms of lineshape accuracy, demonstrate that this should not count against their use.

4. Summary and conclusions

We have generated optimized excitation pulses for static ^{87}Rb solid-state NMR experiments on a sample of $RbClO_4$ at 9.4 T. Such

pulses, which exhibit rapid amplitude and phase modulations, are capable of uniformly exciting the central transition powder pattern, achieving signal enhancements in excess of 100%, and generally resulting in lineshapes much closer to the ideal than the DFS experiment. This is particularly advantageous for static powder patterns, where both EFG and CSA tensor information can be extracted *via* an accurate fit of the lineshape. The observed signal enhancements increase with increasing maximum RF power and increasing pulse lengths, however, optimizations of longer pulses (>30 μs) were found more likely to terminate at locally-optimum solutions.

Perhaps the most exciting aspect of this work is that we have demonstrated the possibility of creating optimized pulses which can achieve excitation and signal enhancement in half-integer quadrupolar systems for which they were not optimized. We have presented a pulse that functions well on three different quadrupolar nuclei with three different spin numbers, with very few experimental parameters needing to be calibrated. This pulse produced full excitation of the lineshapes as well as signal enhancement (albeit far less than the theoretical maximum, especially for the higher spin numbers). We envisage the development of a family of such pulses that will require very little experimental calibration and thus will be extremely useful for studying low sensitivity or low natural abundance quadrupolar nuclei such as ^{17}O or ^{33}S, for which experimental optimization of current enhancement schemes such as DFS may be difficult or time-consuming. Such optimized pulses are also relatively insensitive to transmitter offset and RF power misset when compared with monochromatic pulses or DFS.

The signal enhancement mechanism of these optimized pulses was shown to be markedly different from the DFS scheme, with significant multiple-quantum coherences being created throughout the duration of the pulse, and a non-linear excitation of the satellite-transition manifold, resulting in a more uniform signal enhancement experimentally, particularly in the "magic angle region" of the powder pattern where the satellite transition frequencies of the crystallites are close in proximity to the central transition.

Numerous further developments and applications of these optimized pulses can be imagined. In order to take advantage of the considerable signal enhancement available from the QCPMG experiment [37], these optimized pulses could be used as the initial excitation pulse for this sequence. Optimized broadband refocusing pulses could potentially be of benefit in this application for samples exhibiting relatively wide powder patterns. The signal enhancement arising from these pulses could also be used for C_Q-based spectral editing of static spectra, as recently exemplified using "incomplete" DFS waveforms [38]. Finally, we are currently testing the use of optimized excitation and enhancement pulses for higher spin systems and also MAS conditions, which can increase the sensitivity and spectral resolution significantly.

Acknowledgments

We thank Prof. Thomas Vosegaard (University of Aarhus, Denmark) and an anonymous reviewer for helpful suggestions. The Natural Sciences and Engineering Research Council (NSERC, Canada), the Canadian Foundation for Innovation and the Ontario Innovation Trust are acknowledged for financial support. R.W.S. thanks the Ontario Ministry of Research and Innovation for an Early Researcher Award, and acknowledges the Centre for Catalysis and Materials Research at the University of Windsor for additional funding.

References

[1] S.J. Glaser, T. Schulte-Herbrüggen, M. Sieveking, O. Schedletzky, N.C. Nielsen, O.W. Sørensen, C. Griesinger, Science 280 (1998) 421–424.
[2] N. Khaneja, J.-S. Li, C. Kehlet, B. Luy, S.J. Glaser, Proc. Natl. Acad. Sci. USA 101 (2004) 14742–14747.
[3] N. Khaneja, T. Reiss, C. Kehlet, T. Schulte-Herbrüggen, S.J. Glaser, J. Magn. Reson. 172 (2005) 296–305.
[4] N. Khaneja, F. Kramer, S.J. Glaser, J. Magn. Reson. 173 (2005) 116–124.
[5] D. Stefanatos, S.J. Glaser, N. Khaneja, Phys. Rev. A 72 (2005) 062320.
[6] C. Kehlet, M. Bjerring, A.C. Sivertsen, T. Kristensen, J.J. Enghild, S.J. Glaser, N. Khaneja, N.C. Nielsen, J. Magn. Reson. 188 (2007) 216–230.
[7] C. Kehlet, A.C. Sivertsen, M. Bjerring, T.O. Reiss, N. Khaneja, S.J. Glaser, N.C. Nielsen, J. Am. Chem. Soc. 126 (2004) 10202–10203.
[8] C. Kehlet, T. Vosegaard, N. Khaneja, S.J. Glaser, N.C. Nielsen, Chem. Phys. Lett. 414 (2005) 204–209.
[9] Z. Tošner, S.J. Glaser, N. Khaneja, N.C. Nielsen, J. Chem. Phys. 125 (2006) 184502.
[10] J.Ø. Hansen, C. Kehlet, M. Bjerring, T. Vosegaard, S.J. Glaser, N. Khaneja, N.C. Nielsen, Chem. Phys. Lett. 447 (2007) 154–161.
[11] A.B. Nielsen, M. Bjerring, J.T. Nielsen, N.C. Nielsen, J. Chem. Phys. 131 (2009) 025101.
[12] T. Vosegaard, C. Kehlet, N. Khaneja, S.J. Glaser, N.C. Nielsen, J. Am. Chem. Soc. 127 (2005) 13768–13769.
[13] M. Bak, J.T. Rasmussen, N.C. Nielsen, J. Magn. Reson. 147 (2000) 296–330.
[14] Z. Tošner, T. Vosegaard, C. Kehlet, N. Khaneja, S.J. Glaser, N.C. Nielsen, J. Magn. Reson. 197 (2009) 120–134.
[15] T.E. Skinner, T. Reiss, B. Luy, N. Khaneja, S.J. Glaser, J. Magn. Reson. 163 (2003) 8–15.
[16] T.E. Skinner, T.O. Reiss, B. Luy, N. Khaneja, S.J. Glaser, J. Magn. Reson. 167 (2004) 68–74.
[17] K. Kobzar, T.E. Skinner, N. Khaneja, S.J. Glaser, B. Luy, J. Magn. Reson. 170 (2004) 236–243.
[18] T.E. Skinner, K. Kobzar, B. Luy, M.R. Bendall, W. Bermel, N. Khaneja, S.J. Glaser, J. Magn. Reson. 179 (2006) 241–249.
[19] N.I. Gershenzon, T.E. Skinner, B. Brutscher, N. Khaneja, M. Nimbalkar, B. Luy, S.J. Glaser, J. Magn. Reson. 192 (2008) 235–243.
[20] A.P.M. Kentgens, R. Verhagen, Chem. Phys. Lett. 300 (1999) 435–443.
[21] T. Vosegaard, J. Skibsted, H. Bildsøe, H.J. Jakobsen, J. Phys. Chem. 99 (1995) 10731.
[22] R.W. Schurko, I. Hung, C.M. Widdifield, Chem. Phys. Lett. 379 (2003) 1–10.
[23] C.B. Castellani, O. Carugo, M. Giusti, N. Sardone, Eur. J. Sol. State Inor. 32 (1995) 1089–1099.
[24] A.J. Rossini, R.W. Schurko, J. Am. Chem. Soc. 128 (2006) 10391–10402.
[25] S. Vega, Y. Naor, J. Chem. Phys. 75 (1981) 75–86.
[26] J. Haase, M.S. Conradi, Chem. Phys. Lett. 209 (1993) 287–291.
[27] Z. Yao, H.T. Kwak, D. Sakellariou, L. Emsley, P.J. Grandinetti, Chem. Phys. Lett. 327 (2000) 85–90.
[28] T. Bräuniger, K. Ramaswamy, P.K. Madhu, Chem. Phys. Lett. 383 (2004) 403–410.
[29] R. Siegel, T.T. Nakashima, R.E. Wasylishen, Chem. Phys. Lett. 388 (2004) 441–445.
[30] R. Siegel, T.T. Nakashima, R.E. Wasylishen, Concept. Magn. Reson. A 26 (2005) 47–61.
[31] L.A. O'Dell, R.W. Schurko, J. Am. Chem. Soc. 131 (2009) 6658–6659.
[32] J.-S. Lee, R.R. Regatte, A. Jerschow, J. Chem. Phys. 129 (2008) 224510.
[33] J.-S. Lee, R.R. Regatte, A. Jerschow, J. Chem. Phys. 131 (2009) 174501.
[34] R. Siegel, T.T. Nakashima, R.E. Wasylishen, J. Magn. Reson. 184 (2007) 85–100.
[35] L.A. O'Dell, R.W. Schurko, Chem. Phys. Lett. 464 (2008) 97–102.
[36] N.M. Trease, K.K. Dey, P.J. Grandinetti, J. Magn. Reson. 200 (2009) 334–339.
[37] F.H. Larsen, H.J. Jakobsen, P.D. Ellis, N.C. Nielsen, J. Phys. Chem. A 101 (1997) 8597–8606.
[38] X. Wang, L.J. Smith, Solid State Nucl. Magn. Reson. 36 (2009) 99–102.